



RESEARCH ARTICLE

10.1029/2023SW003748

Special Section:

Starlink Satellite Losses during the February 2022 Geomagnetic Storm Event: Science, Technical and Economic Consequences, Policy, and Mitigation

Key Points:

- Ionospheric field-aligned current and thermospheric neutral densities are examined for the 2022 Starlink geomagnetic storms
- The field-aligned currents changed quickly, whilst the density decayed slowly and with differing timescales
- Asymmetric latitudinal density distributions are consistent with asymmetries in the field aligned currents

Correspondence to:

D. D. Billett,
ddb524@mail.usask.ca

Citation:

Billett, D. D., Sartipzadeh, K., Ivarsen, M. F., Iorfida, E., Doornbos, E., Kalafatoglu Eyiguler, E. C., et al. (2024). The 2022 Starlink geomagnetic storms: Global thermospheric response to a high-latitude ionospheric driver. *Space Weather*, 22, e2023SW003748. <https://doi.org/10.1029/2023SW003748>







Received 29 SEP 2023

Accepted 22 JAN 2024

© 2024. The Authors.

This is an open access article under the terms of the [Creative Commons Attribution-NonCommercial-NoDerivs License](https://creativecommons.org/licenses/by-nc-nd/4.0/), which permits use and distribution in any medium, provided the original work is properly cited, the use is non-commercial and no modifications or adaptations are made.

The 2022 Starlink Geomagnetic Storms: Global Thermospheric Response to a High-Latitude Ionospheric Driver

D. D. Billett¹ , K. Sartipzadeh^{1,2}, M. F. Ivarsen^{1,3} , E. Iorfida⁴ , E. Doornbos⁵ , E. C. Kalafatoglu Eyiguler¹, K. Pandey¹ , and K. A. McWilliams¹ 

¹Institute of Space and Atmospheric Studies, University of Saskatchewan, Saskatoon, SK, Canada, ²University of Tromsø (UIT)—The Arctic University of Norway, Tromsø, Norway, ³Department of Physics, University of Oslo, Oslo, Norway, ⁴Aurora Technology B.V. for European Space Agency (ESA), ESTEC, EOP-SME, Noordwijk, The Netherlands, ⁵Royal Netherlands Meteorological Institute (KNMI), De Bilt, The Netherlands

Abstract In this study, we present ionospheric observations of field-aligned currents from AMPERE and the ESA Swarm A satellite, in conjunction with high-resolution thermospheric density measurements from accelerometers on board Swarm C and GRACE-FO, for the third and 4 February 2022 geomagnetic storms that led to the loss of 38 Starlink internet satellites. We study the global storm time response of the thermospheric density enhancements, including their decay and latitudinal distribution. We find that the thermospheric density enhances globally in response to high-latitude energy input from the magnetosphere-solar wind system and takes at least a full day to recover to pre-storm density levels. We also find that the greatest density perturbations occur at polar latitudes consistent with the magnetosphere-ionosphere dayside cusp, and that there appeared to be a saturation of the thermospheric density during the geomagnetic storm on the fourth. Our results highlight the critical importance of high-latitude ionospheric observations when diagnosing potentially hazardous conditions for low-Earth-orbit satellites.

Plain Language Summary Upwards of a 100 km altitude lies the boundary between Earth's atmosphere and space, where the density of air exponentially decreases and many satellites constellations orbit. One of these constellations is Starlink, which provides satellite internet to customers on Earth. In February 2022, a pair of geomagnetic storms struck Earth shortly after the launch of 49 Starlink satellites, heating the upper atmosphere and causing its density to drastically increase. The higher air density at the initial staging altitude of Starlink caused fatal drag conditions for 38 of the spacecraft, resulting in their destruction a few days later. This paper examines how the air density of the upper atmosphere changed globally in response to space weather energy being deposited at high latitudes during the Starlink geomagnetic storms of February 2022.

1. Introduction

In February 2022, 38 Starlink internet satellites were destroyed shortly after launch as a result of two back-to-back geomagnetic storms on the 3rd and 4th of that month. These storms carried with them an increase to the amount of Poynting flux entering the high-latitude ionosphere of both hemispheres (e.g., C. Y. Huang et al., 2017), leading to Joule heating and a subsequent perturbation of the thermospheric mass density at low-Earth-orbit (LEO) altitudes (Deng et al., 2009; Wang et al., 2021). Whilst the two storms did ultimately lead to increased thermospheric densities and dangerous orbital drag conditions for Starlink, they would not be considered “extreme,” or even “strong,” space weather events, as we demonstrate below. The thermosphere experienced a moderate amount of geomagnetic forcing at high-latitudes, which in turn propagated high densities globally, causing the hazardous conditions at Starlink's staging altitude of ~200 km (Berger et al., 2023; Dang et al., 2022; Fang et al., 2022; Hapgood et al., 2022; Laskar et al., 2023; Lin et al., 2022). The satellites burned up in Earth's atmosphere on 7 February 2022.

Not only does increased drag lead to potential launch failures such as that seen in February 2022, but it also affects precise orbit determination, satellite lifespans, and collision avoidance (He et al., 2018; Oliveira & Zesta, 2019). As LEO altitudes become more congested with satellite infrastructure, the density of the thermosphere becomes increasingly important to understand. Higher than expected densities, due to geomagnetic storms more extreme than that which led to the Starlink destruction event, could cause premature satellite re-entry,

or satellite-on-satellite collisions, due to orbit prediction inaccuracies (Zesta & Oliveira, 2019). Geomagnetic storms therefore threaten sustainability across the LEO satellite industry, from launch through to operations.

The thermospheric effects of the Starlink storms, like other moderate geomagnetic storms, start at Earth's high-latitude ionosphere. Field-aligned-currents (FACs) channel solar wind electromagnetic energy into the ionosphere via magnetospheric reconnection events (e.g., the Dungey cycle; Dungey, 1961), which dissipates through Pedersen currents as Joule heating (Foster et al., 1983). As Joule heating is mostly deposited at E-region altitudes where the Pedersen conductivity is highest (Y. Huang et al., 2012), density perturbations at LEO altitudes are mostly generated by the upwelling of neutral particles and expansion of the thermosphere due to heating pressure from below (Lu et al., 2016). Traveling atmospheric disturbances (TADs) propagate from high to low latitudes as increased pressure drives an equatorward meridional wind (Pröls & Očko, 2000), acting as a vehicle for perturbing globally the thermospheric density (Pröls, 2011).

On 31 January 2022, the Space Weather Prediction Center (SWPC) at the National Oceanic and Atmospheric Administration (NOAA) issued a geomagnetic storm warning for the coming days (<https://www.swpc.noaa.gov/news/geomagnetic-storm-conditions-likely-2-3-february-2022>, updated 3 February). The predicted as well as the actual magnitudes of the storms on 3 and 4 February were minor, as was the thermospheric density perturbations they drove, yet they were sufficient to cause major damage to Starlink assets shortly after their launch. Fang et al. (2022) points out that although commercial space operators have access to NOAA space weather predictions, none of those predictions at the time of the Starlink event focused on the orbital drag effects relating to thermospheric density enhancements. Whilst engagement between industry and space weather prediction services improves, understanding the magnetosphere-ionosphere driving conditions behind thermospheric density perturbations is vital for said predictions to be both accurate and precise. Therefore in this study, we present a global scale analysis of ionospheric and thermospheric observations during the February 2022 Starlink geomagnetic storms.

As a measure of the space weather input into the atmosphere, we show FAC measurements from the Active Magnetosphere and Planetary Response Experiment (AMPERE) and Swarm A satellite. For the thermospheric densities, we employ newly processed high-resolution accelerometer measurements from Swarm C and GRACE-FO. Of particular interest is understanding the global extent of thermospheric perturbations in response to a high-latitude ionospheric driver, investigating the growth and decay of density perturbations, as well as their latitudinal distribution.

2. Data

2.1. Thermospheric Densities From Swarm-C and GRACE-FO

Thermospheric densities in this study were obtained from the Swarm and Gravity Recovery And Climate Experiment Follow On (GRACE-FO) missions (Friis-Christensen et al., 2008; Kornfeld et al., 2019). In particular, densities used are derived from accelerometers on board Swarm C at an approximate altitude of 450 km and GRACE C at ~500 km. Both satellites fly in a near-polar orbit with inclinations of 87.4° and 89°, respectively. Although calibration errors for both Swarm and GRACE-FO accelerometers are not provided in the level 2 thermospheric density product, the accelerometer cross-track winds generally have an error of a few n ms^{-1} (Bezděk et al., 2018). The uncertainty of the densities, however, are described as “30% of variance of orbit average of mass density or $5 \times 10^{-14} \text{ kg m}^3$, whichever value is largest” (see “Swarm Level 2 Processing System Product specification for L2 Products and Auxiliary Products”).

The ESA Swarm satellites are the 4th ESA Earth Explorer mission, which was launched in November 2013. They are a constellation of three identical satellites flying at different altitudes. For all three of the Swarm satellites (A, B, and C), calibration of the raw accelerometer measurements has proven difficult due to unforeseen and/or underestimated non-geophysical perturbations (Siemes et al., 2016). Swarm C proved to contain the least number of disturbances and strongest signal-to-noise ratio of the three satellites, thus making it the primary focus of neutral density retrieval efforts over the years. Additionally, densities derived from on-board GPS observations, at a low temporal resolution, have helped greatly in higher-resolution accelerometer calibration efforts (Visser & van den IJssel, 2016; van den IJssel et al., 2020). Swarm C accelerometer measurements now provide good thermospheric density estimations at a 10 s temporal resolution, allowing for high-latitude density perturbations to be effectively decoupled from those low latitudes. We therefore utilize Swarm C accelerometer derived thermospheric densities

in this study, as they provide a vast spatio-temporal resolution improvement over GPS densities and allow for the effects of high-latitude geomagnetic energy input to be investigated more rigorously (Iorfida et al., 2023).

GRACE-FO, the successor to the GRACE mission (Tapley et al., 2004) on near-identical hardware, is a twin-satellite mission launched in 2018. Recently, GRACE-FO accelerometer measurements for satellite C of the pair (the other being GRACE D, which unfortunately produced poorer accelerometer data after launch; McCullough et al., 2019) have been released (Siemes et al., 2023), building upon nearly two decades of calibration efforts for the original GRACE, CHALLENGING Mini satellite Payload (CHAMP), and Gravity Field and Steady-State Ocean Circulation Explorer (GOCE) satellites (Bruinsma et al., 2004; Doornbos, 2012; March et al., 2021; Mehta et al., 2017). Like Swarm C, thermospheric densities from GRACE-FO are at a 10 s temporal resolution.

2.2. Field Aligned Currents From Swarm a and AMPERE

We utilize FAC measurements from the AMPERE campaign (Anderson et al., 2014) and Swarm A satellite. FAC's carry the Poynting flux that is mostly dissipated as Joule heating in the atmosphere (Billett et al., 2023), thus their magnitude and spatial extent act as a key parameter in evaluating high-latitude ionospheric driving of any potential thermospheric density enhancements.

Swarm A flies as a satellite pair with Swarm C at the same altitude, separated by 1.4° in longitude. FAC estimations are derived from the on-board vector fluxgate magnetometer (Leger et al., 2009) utilizing Ampère's law along with models to remove the background magnetic field component (Lühr et al., 2015). The Swarm FAC data product has a temporal resolution of 1 s, upon which we apply running mean and Savitsky-Golay filters with 20 s half-window sizes to remove small-scale perturbations and noise.

AMPERE produces high-latitude FAC estimations based on magnetometer observations from the Iridium communications constellation. FAC estimates are available on a 1-degree geomagnetic latitude by 1 hr magnetic local time grid, sampled from a spherical harmonic fit applied to available magnetometer measurements (after subtraction of Earth's main field) (Waters et al., 2020). AMPERE FAC maps are produced at a nominal 10-min resolution. For the purposes of comparing Swarm A and AMPERE data later in this paper, the AMPERE time intervals shown correspond to average polar pass time of Swarm A, rounded to the nearest 10 min.

3. Results and Discussion

3.1. Thermospheric Density Response and Decay

Figure 1 presents an overview of the days surrounding the Starlink satellite launch on 3 February 2022. The top panel shows the 1-min geomagnetic SYM-H index, obtained from NASA's OMNIWeb service, whilst panels (a) and (b) show the thermospheric neutral densities measured by GRACE-FO and Swarm C, respectively. The neutral densities are shown in terms of Altitude Adjusted Corrected Geomagnetic (AACGM; Shepherd, 2014) latitude versus time, with periodic gaps near $\pm 90^\circ$ illustrating the offset of the geomagnetic pole from that of the geographic in both hemispheres. As both GRACE-FO and Swarm C have near-polar orbits in geographic coordinates, coverage above $\pm 80^\circ$ AACGM latitude is poorer in the southern hemisphere compared to north. As AACGM coordinates are not defined for equatorial latitudes, latitudes between -15° and $+15^\circ$ are not considered. Note that each "half orbit" is shown sequentially, giving the appearance of periodic increases and decreases of the neutral density as the satellite crosses the dayside (higher density), and then the nightside (lower density). GRACE-FO data was unavailable on 2 February 2022. The Starlink launch on 3 February 2022 was at 18:32, as indicated by the vertical dashed line.

The SYM-H index shown in Figure 1 displays a distinct negative excursion to ~ -80 nT on 3rd February 2022, the day of the Starlink launch. Storm magnitude classifications vary greatly within the literature, however, a storm of SYM-H magnitude as seen during this event would be generally considered "weak" or "moderate" (Hutchinson et al., 2011; Iong et al., 2022; Richardson & Cane, 2012). Concurrent with the 3rd February storm are global scale enhancements of the thermospheric neutral density, captured by both GRACE-FO and Swarm C at altitudes of ~ 500 and ~ 460 km, respectively. Note that the color scales on Figures 1a and 1b are different, owing to the normal exponential drop of neutral density with increasing altitude in the thermosphere. The peak neutral density, seen by both GRACE-FO and Swarm C, is at around 80° AACGM latitude in the northern hemisphere. We

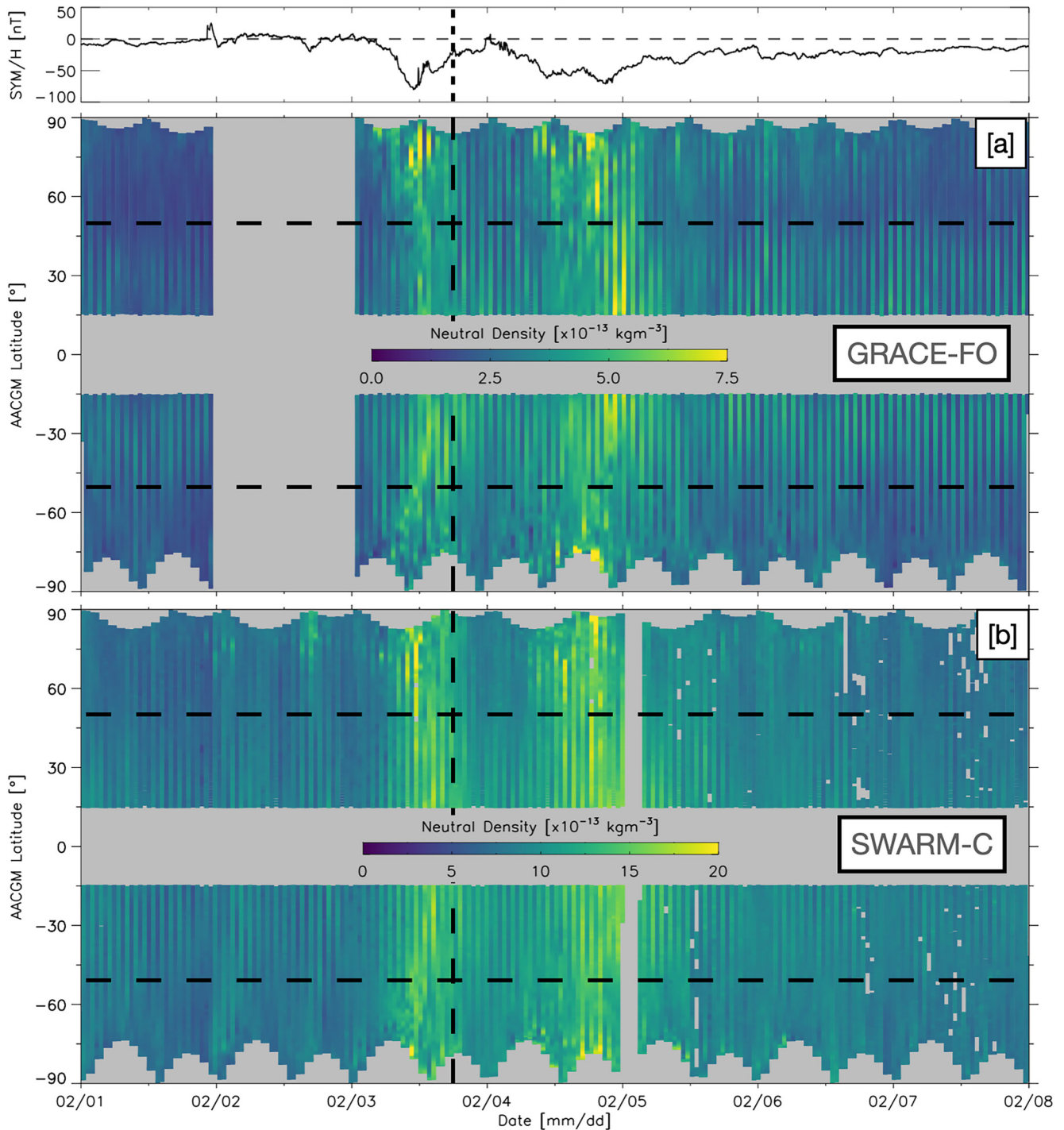


Figure 1. Thermospheric conditions between 1st and 7th February 2022. [Top] 1-min SYM-H index, (a) Thermospheric neutral density as a function of AACGM latitude and time from GRACE-FO, (b) Densities from Swarm C. The vertical dashed line indicates the time of the Starlink launch on 3 February, and the horizontal dashed lines constrain the approximate AACGM latitude range of the satellites launched (based on two-line element data from <https://www.space-track.org/>).

attribute this high latitude density peak to geomagnetic energy input from the magnetosphere in the form of Joule heating into the ionospheric cusp region (Billett et al., 2021; Knipp et al., 2011; Lühr et al., 2004).

A second geomagnetic storm, longer lasting than the one on 3rd February but of a similar SYM-H magnitude, occurred on 4th February 2022, 1 day after the Starlink launch. There is another global response of the thermospheric neutral density on the 4th, including an equatorward motion of density enhancements from high northern

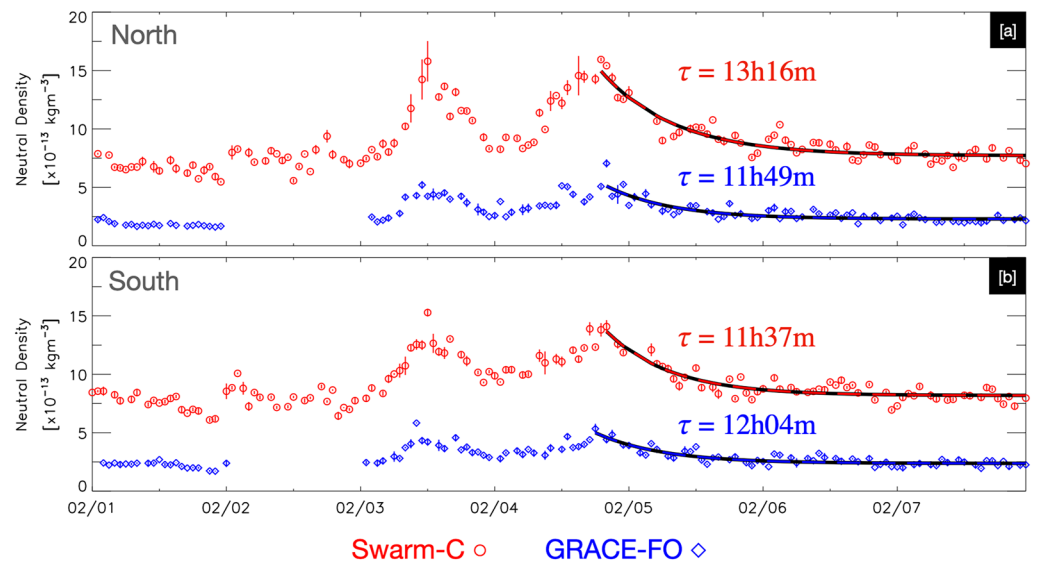


Figure 2. Mean thermospheric neutral densities between 60° and 70° AACGM latitude from 1st and 7th February 2022, measured by GRACE-FO and Swarm C. (a) Northern hemisphere, (b) Southern hemisphere. Exponential decay curves are fitted from the second peak of each time series onwards, with e-folding times for each shown. Error bars lines are also shown, representing the standard deviation of each mean point.

and southern latitudes over the course of the day, most apparent in the GRACE-FO measurements. This motion is consistent with TAD propagation, and modeling of the same event (Laskar et al., 2023; Lin et al., 2022). Overall, thermospheric densities were significantly higher within the latitude bounds of the initial Starlink orbit (horizontal dashed lines in Figure 1) on the 4th, compared to the 3rd. The two geomagnetic storms on the 3rd and 4th are consistent with the passing of two CME-associated magnetic clouds which passed Earth, following solar flares on 30 January 2022 and 1 February 2022 (Dang et al., 2022).

To evaluate the growth and decay of the thermospheric neutral density in response to the geomagnetic storms of the 3rd and 4th February 2022, Figure 2 shows the hourly averaged densities from GRACE-FO and Swarm C between 60° and 70° AACGM latitude, in the northern [a] and southern [b] hemispheres, respectively. The latitude range was chosen to ensure similar satellite coverage in both hemispheres (owing to the poorer polar coverage in the south), whilst being at a latitude high enough to capture magnetospheric energy inputs due to the geomagnetic storms (i.e., the auroral zone) reasonably soon after they occur. The curves from 4th February onwards are exponential decay least-square fits in the form $\rho(t) = ae^{-t/\tau} + b$, where $\rho(t)$ is the neutral density as a function of time, a and b are fit constants, and τ is the e-folding time. τ is strictly the time taken for the thermospheric density to decrease by a factor of $1/e$, which we use as representative of the time required for the thermosphere to “recover” after the geomagnetic storm on 4th February. The root-mean-square errors (RMSE) of the exponential fits, as a percentage of the mean of the data that was fitted, are 7.6%/6.7% for Swarm (north and south, respectively), and 15.9%/11.8% for GRACE-FO.

Both GRACE-FO and Swarm C measured two distinct neutral density peaks in the auroral zones of both hemispheres (Figures 2a and 2b), in response to the geomagnetic storms on the 3rd and 4th February 2022. These time series, averaged over the latitude range 60–70°, are broadly similar to the global orbit averaged time series shown by Lin et al. (2022) for Swarm A, as well as the MAGE, TIEGCM, and DTM model outputs. The storm-time density in this latitude range was 1.9% and 2.8% higher in the southern hemisphere compared to the north at GRACE-FO and Swarm C altitudes, respectively. This hemispheric difference is rather small considering that the southern hemisphere is in local summer, which should result in a significantly larger overall density than the winter (northern) hemisphere (Ercha et al., 2012). It has previously been seen that there is a northern hemisphere preference for increased magnetospheric energy input when compared to the south (Pakhotin et al., 2021), which would result in a density asymmetry due to Joule heating.

Other hemispheric asymmetries in Figure 2 are present. For example, the density trough around midnight on the 4th of February between the two storm peaks is deeper in the northern hemisphere compared to the south for the

same spacecraft. This would imply a quicker decay time for the enhanced neutral density to return to background levels in the northern hemisphere after the storm on 3rd February. τ values calculated from the peak of the 2nd storm onwards, however, do not indicate a faster northern hemisphere recovery for the second storm. τ varies between spacecrafts and hemispheres, ranging from 11h37 to 13h16 m, but the decay time from Swarm C in the northern hemisphere is significantly longer than the rest, which vary by around 30 min τ for Swarm C in the north is 1 hr 12 min longer than the next closest τ , which could mean that the density perturbation in the northern hemisphere around 460 km is larger than that in other regions, that the thermosphere there is more “sluggish” in returning to pre-storm levels, or a combination of both conditions. As SYM-H takes several days to return to values near zero after the storm on 4th February (Figure 1), it is also possible there is persistent Joule heating that lingers and causes the neutral density to not fully return to quiet-time levels (Zhou et al., 2007). We note that because the RMSE of the exponential fit for Swarm in the northern hemisphere was 7.6% (approximately 1 hr error in τ), its longer e-folding time may be within error tolerances of the others. The apparent quick thermospheric decay time after the first storm, on 3rd February, may be due to enhanced nitric oxide cooling associated with coronal mass ejection (CME) driven storms (Knipp et al., 2017; Licata et al., 2022), although an exact τ cannot be determined due to the onset of the second storm. Overall decay times presented here are consistent with those presented in the statistical study by Zesta and Oliveira (2019), and likely vary somewhat with local time (e.g., Weimer et al., 2023).

3.2. Disturbance Thermospheric Densities and Ionospheric Drivers

We now discuss the high-latitude ionospheric conditions responsible for driving the globally enhanced thermospheric densities on the 3rd and 4th February 2022. Figures 3a and 3c shows neutral density measurements from GRACE-FO and Swarm C on 3rd February 2022, accompanied by estimations of the “quiet time” density from the Naval Research Laboratory Mass Spectrometer Incoherent Scatter radar model (NRLMSIS 2.0, shortened to “MSIS” in this study; Emmert et al., 2021). $A_p = 3$ as MSIS input was chosen to represent “quiet” geomagnetic conditions for the purpose of this study (Joselyn, 1989), which was found to closely resemble the GRACE-FO and Swarm C measurements on the 2 days prior to the 3rd of February storm. As MSIS is an empirical model based on averaged thermospheric data sets from various sources, it is an excellent tool in this scenario to determine how much the Swarm-C and GRACE-FO measurements deviate from average quiet time conditions along the satellite track. Figures 3b and 3d show perturbation neutral densities derived by subtracting the quiet time MSIS estimations from the satellite measurements. Orbit averaged perturbation densities are additionally shown here, calculated using a running mean window of size equal to the respective satellites orbital period. Figures 3e and 3f show FAC measurements from AMPERE along dusk-dawn latitude slices in both the northern and southern hemispheres, respectively. Finally, Figure 3g shows a snapshot of the global AMPERE and local Swarm A FAC measurements during the shaded interval. Overlain black arrows are Swarm A's trajectory over the northern and southern hemisphere high-latitude regions, extending to 50° colatitude (40° AACGM latitude). Swarm A data is shown both as colored circles over the AMPERE data, as well as a time series. Blue (negative) FAC values are downward (into) in the northern hemisphere and upward (out of) in the south, and vice versa for red.

The negative excursion of SYM-H signifying the start of the storm on 3rd February (Figure 1) begins at ~05:00UT. It is from approximately then that the neutral density measurements from GRACE-FO and Swarm C begin to deviate from MSIS estimations (Figures 3a and 3c). Other than the deviation from quiet time baselines, MSIS appears to capture latitudinal and local time variability of the satellite densities well. The deviation is clearer in the perturbation densities (Figures 3b and 3d), showing that those at both ~460 and ~500 km altitude reach an orbit average maximum at 11:40 UT and 12:40 UT, respectively. The perturbation densities also reveal that both GRACE-FO and Swarm C measure peaks at around the same time, within the highlighted region at 12:00 UT, giving a time lag of ~7 hr between storm onset and peak density perturbation. The maximum single-point perturbation density measurement and orbit averaged perturbation density was 380%/96% for GRACE-FO (a factor increase 4.8 and 1.96), respectively, and 260%/84% (3.6/1.84) for Swarm C. We note that although the maximum orbit averaged density perturbation presented here is similar to that determined by other studies for the Starlink storms (between 50% and 100% based on modeling and orbit averaged data; Lin et al., 2022; Dang et al., 2022), the moment-to-moment densities at both GRACE-FO and Swarm C altitudes often greatly exceed the average, especially at high latitudes.

A more direct way of measuring the ionospheric activity in response to geomagnetic storms, versus the SYM-H index, is by observing the magnitude and latitudinal extent of the global scale FAC system. The progression of

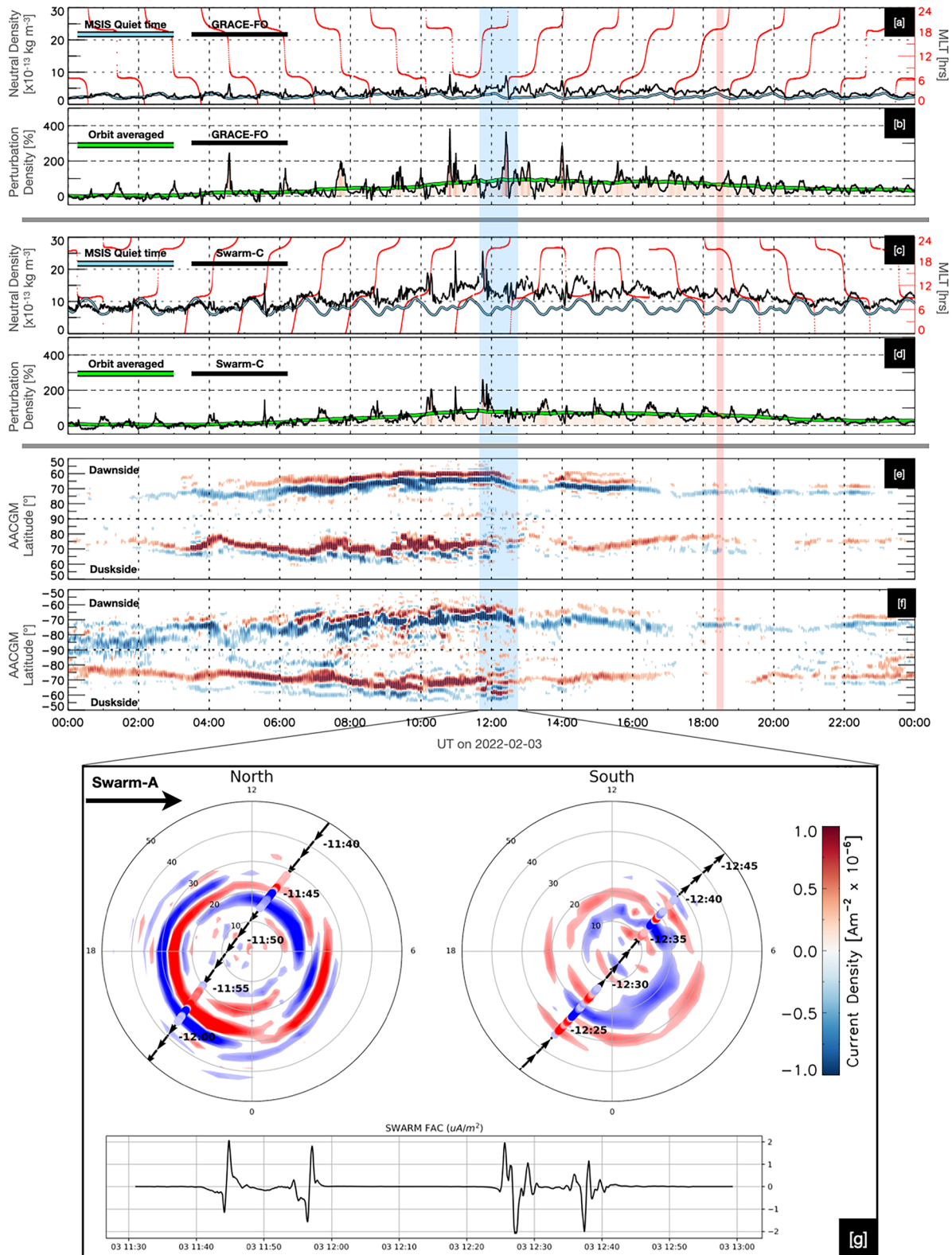


Figure 3. Thermosphere/ionosphere conditions on 3 February 2022. (a) and (c): Time series of measured thermospheric densities from GRACE-FO (a) and Swarm C (c), with MSIS quiet time estimations (blue) and the magnetic local time of the spacecraft (red). (b) and (d): Perturbation thermospheric densities from GRACE-FO (b) and Swarm C (d), with orbit averaged values underlain. (e) and (f): Latitude slice keograms of the dusk-dawn (bottom to top) FACs observed by AMPERE for the northern (e) and southern (f) hemispheres, where negative (blue) and positive (red) values signify currents into and out of the atmosphere, respectively. (g): AMPERE and Swarm A FAC measurements from within the shaded region. The vertical red shaded region indicates the time of the Starlink launch.

the dusk and dawn FACs, in both hemispheres, is thus shown in Figures 3e and 3f. From the beginning of the day till around 12:00 UT, there was a consistent and gradual equatorward expansion of the R1 and R2 FACs, on both the dawn and dusk sides and in both hemispheres. This expansion is typical of geomagnetic storm growth phases, where the high-latitude Dungey cycle system reaches lower latitudes as increasing amounts of flux enter the polar cap due to magnetopause reconnection, that is, the expanding-contracting-polar-cap paradigm (Cowley & Lockwood, 1992). 12:00 UT also approximately coincides with the maximum extent of SYM-H (Figure 1), and is thus a good time to designate as the storm main phase “end.” The ~ 7 hr lag of the peak neutral density (and has seen here, the peak FAC magnitude) to the start of the main phase is consistent with statistics of geomagnetic storm main phase duration (Yokoyama & Kamide, 1997).

After around 12:00 UT, the thermospheric densities measured by GRACE-FO and SWARM-C decrease along with magnitude of the FACs measured by AMPERE. The FACs, however, decrease in magnitude much faster than the densities and retreat poleward, particularly in the southern hemisphere (panel f). The FACs on the northern hemisphere (panel e) dawnside remain intense till $\sim 16:00$ UT, before finally diminishing similar to the southern hemisphere. The slow decay timescales of the neutral densities (panels a–d) after the peak of the storm around 12:00 UT is put into stark contrast with the decay of the FACs, which diminish drastically faster.

As the magnitude of the FACs are related to the horizontal perturbation of the ionospheric magnetic field, and thus the Poynting flux, Joule heating into the ionosphere-thermosphere system on 3 February 2022 increased up to a maximum globally around 12:00 UT. The asymmetry between northern and southern hemisphere FACs (Figures 3e and 3f) implies a northern hemisphere preference for Poynting flux energy input (in agreement with Pakhotin et al., 2021), which is surprising given that the northern (southern) hemisphere was in local winter (summer) at the time. There is thus further evidence for a magnetospheric driver to the aforementioned perturbation density asymmetry, which may ultimately be due to geomagnetic field and conductance differences between the two hemispheres (Cosgrove et al., 2022).

AMPERE and Swarm A FACs are shown in Figure 3g for the shaded interval in panels a–f, roughly coinciding with the time of peak perturbation density and FAC magnitude. AMPERE and Swarm A are in good agreement with each other. The northern hemisphere FAC pattern extended further equatorward than in the south and contained higher current magnitudes. The northern hemisphere FAC is more akin to a “classical” FAC picture than the south, with clearly structured R1 and R2 currents on both the dawn and dusk sides (Iijima & Potemra, 1978).

Figures 4a–4g shows thermosphere–ionosphere conditions for 4th February 2022, 1 day after the Starlink launch and the day of the second geomagnetic storm. The SYM-H onset of this storm was at approximately 01:00 UT, with a peak negative excursion reached at $\sim 21:00$ UT (Figure 1). The start and end of the SYM-H variance on the 4th corresponds well with the magnitude of AMPERE measured FACs (Figures 4e and 4f), which also begins to enhance at 01:00 UT and peak around 21:00 UT. The peak perturbation neutral density observed by both GRACE-FO and Swarm C, however, occurred around 19:00 UT, an 18 hr lag from storm onset and 2 hr before the end of the main phase (according to both SYM-H and AMPERE). It is interesting that the peak perturbation density on the 4th occurred 1–2 hr before the peak SHM-H negative excursion, as it implies there is perhaps a thermospheric density “saturation” point that is based on the duration of the storm main phase, and/or the magnitude of the storm itself.

The peak single-point perturbation density measurement and orbit averaged perturbation density was higher on the 4th compared to the 3rd, 476%/125% (factor increases of 5.76 and 2.25) respectively for GRACE-FO. Swarm C measured several very large density perturbations over a 5-min period at 18:50 UT which were not flagged as anomalous in the data quality flags, resulting in a maximum single-point perturbation density measurement of 510% (factor 6.1 increase). We treat this as anomalous as the maxima during the preceding and proceeding peaks were under 200% (3.0), and because the thermospheric density is highly unlikely to vary by so much so quickly. The peak orbit-averaged perturbation density measured by Swarm C was 107% (2.07) (excluding anomalous points), higher than that seen on the 3rd of February.

The orbit averaged densities from GRACE-FO and Swarm C were considerably higher on the 4th of February compared to the 3rd, by 29% and 23%, respectively. We attribute this difference to the global extent of density enhancements that each storm produced. Figure 1a shows that the storm on the 4th resulted in density perturbations propagating from high to low latitudes, increasing the density significantly there. On the 3rd, however,

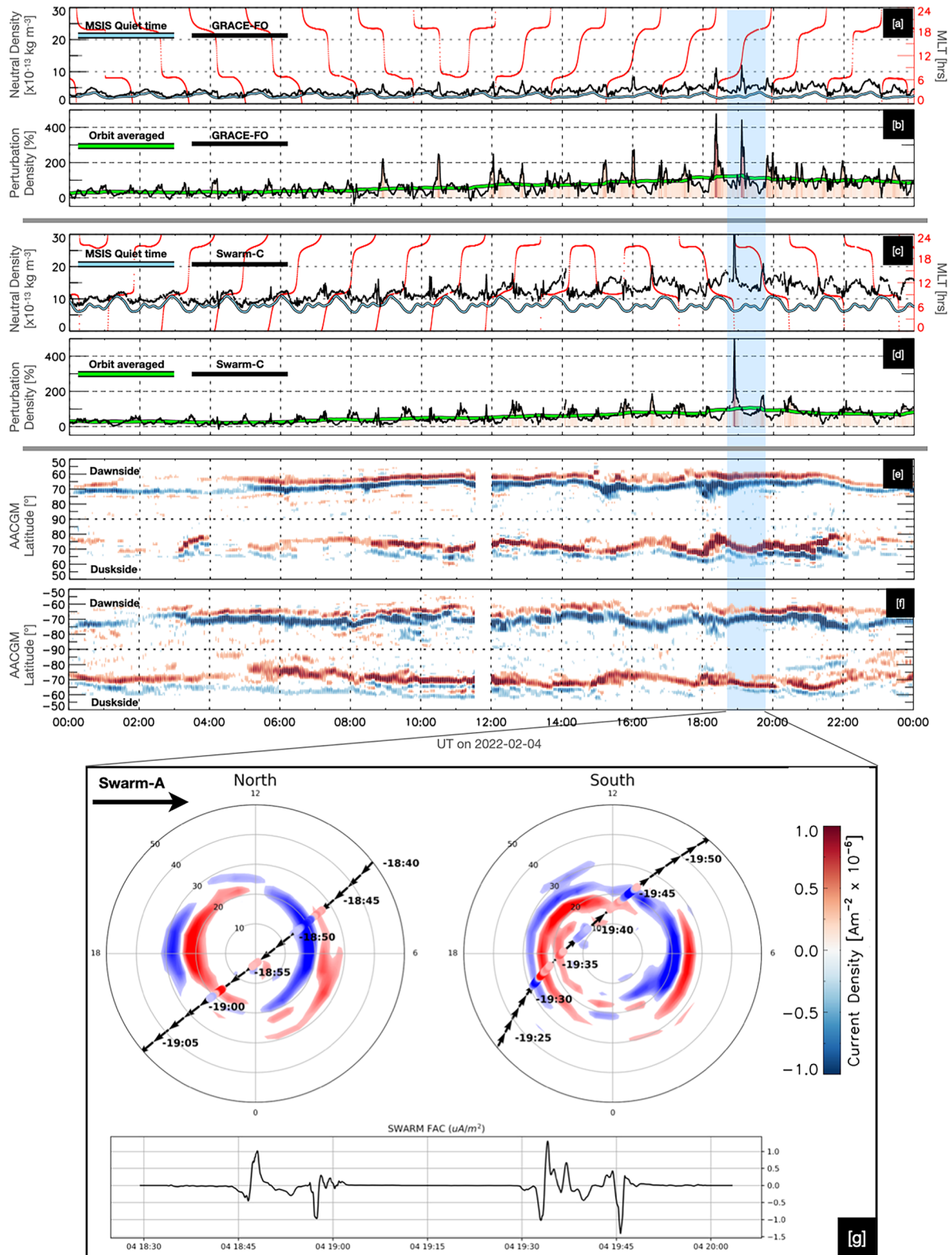


Figure 4. Same format as Figure 3, but for 4th February 2022.

the low-to-mid latitude neutral density was significantly lower, compared to the 4th. The difference in global densities between the 2 days may be related to the aforementioned FAC asymmetry (Figures 3e–3g). On the 4th, the northern and southern hemisphere FACs observed by AMPERE and Swarm A are more symmetric (Figures 4e–4g), which would result in more symmetric Joule heating, and thus a more symmetric distribution of density enhancements and TAD propagation. The latter causes an “intersection” of TADs at low latitudes, driving significant density enhancements there (e.g., those seen on the 4th February in Figure 1; Pham et al., 2022). Thus, the asymmetric FACs on the 3rd would produce asymmetric TAD propagation, in agreement with recent modeling work (Hong et al., 2023; Zhu et al., 2023).

Figure 5 is in the same format as Figures 3 and 4, but showing the 5th of February 2022 (the day after the second storm, 2 days after the Starlink launch). There were no additional storms on this day according to the SYM-H index (Figure 1), and the FACs measured by AMPERE were significantly diminished in both hemispheres compared to the previous 2 days. AMPERE and Swarm A FACs are shown for the highlighted times around 04:30 UT (Figure 5g), showing that the FAC equatorward extent and magnitude were indeed drastically reduced compared to the previous two storm days, although we do note that the currents were generally stronger in the southern hemisphere. FAC reconfiguration timescales after changes in solar wind driving, and in turn Joule heating reconfiguration times, are typically on the order of 10–150 min (Anderson et al., 2018; Billett, McWilliams, Perry, et al., 2022; Coxon et al., 2019), which is consistent with our observations here.

The densities observed by GRACE-FO and Swarm C gradually decreased throughout the 5th February 2022 (Figures 5a–5d), eventually returning close to the MSIS quiet-time baseline by days end. As shown in Figure 2, the neutral density after the second geomagnetic storm was characterized by an e-folding time of around 12 hr, which is in stark contrast to the much faster decay of the enhanced FACs from the previous day (Figures 4e–4g). We noted earlier that there was a similar fast FAC decay and slow thermospheric density decay seen on the 3rd (Figure 3), but the densities on the 3rd did not return to quiet time values due to the onset of the 4 February geomagnetic storm.

Finally, we investigated the latitudinal dependence of the perturbation thermospheric density by creating daily mean profiles versus latitude, shown in Figure 6 from 1st to 7th February 2022. The 7th of February is the date on which the failed Starlink satellites burned up on re-entry.

The largest perturbation densities were seen on storm days (Figures 6c, 6d, 6j, and 6k), with larger perturbations seen by GRACE-FO compared to Swarm C (500 km/460 km average altitude, respectively). GRACE-FO measured maximum mean perturbations of 110% and 131% (factor increases of 2.1 and 2.31) on the 3rd and 4th respectively, compared to Swarm C measurements of 80% and 86% (1.8 and 1.86). Maximums from both satellites were in the northern hemisphere, at polar cap latitudes between 75° and 85°. These latitudes are considerably higher than typical auroral latitudes of ~65°–70°, implying that the peak magnetospheric energy input into atmosphere for these storms is occurring on open magnetic field lines, or close to the open-closed field line boundary. This is a similar result to those presented by R. Liu et al. (2010), C. Y. Huang et al. (2014), Shi et al. (2017), and Wang et al. (2021), who all saw large geomagnetic storm-associated thermospheric density enhancements occurring well within the polar cap. These enhancements have been attributed to Joule heating in the region of enhanced cusp Alfvénic electric fields and are likely related to the development of the “cusp density anomaly” (Lotko & Zhang, 2018; Lühr et al., 2004). The latitudinal width of density enhancements were also smaller in the southern hemisphere compared to north, which is consistent with the statistical distribution of the cusp density anomaly in both hemispheres (H. Liu et al., 2005). Finally, we note that the latitudinal profiles of the mean perturbation densities are not substantially different between GRACE-FO at ~500 km altitude and Swarm-C at ~450 km altitude. The lack of difference is unsurprising, as the thermospheric scale height is not likely to vary much in 50 km (Doornbos, 2012; Newton & Pelz, 1973).

Although Joule heating would require knowledge of the ionospheric conductivity and electric field, and the thermospheric neutral wind, AMPERE has previously been used to estimate the Poynting flux with complementary electric field data from the Super Dual Auroral Radar Network (SuperDARN; Billett, McWilliams, Perry, et al., 2022). It was found, however, that the large scale electric field fit from SuperDARN was too smoothed out spatiotemporally to capture the small- and mesoscale variability of the system. The electric field instrument on board the Swarm satellites can be used in conjunction with AMPERE (or the on board magnetometer) to calculate the Poynting flux, at suitably small scales to capture the Alfvénic variability which drives the cusp density enhancement (Billett, McWilliams, Pakhotin, et al., 2022), but this can only be carried out during certain events where errors in the along-track ion drift measurements can be minimized (Billett et al., 2023; Lomidze

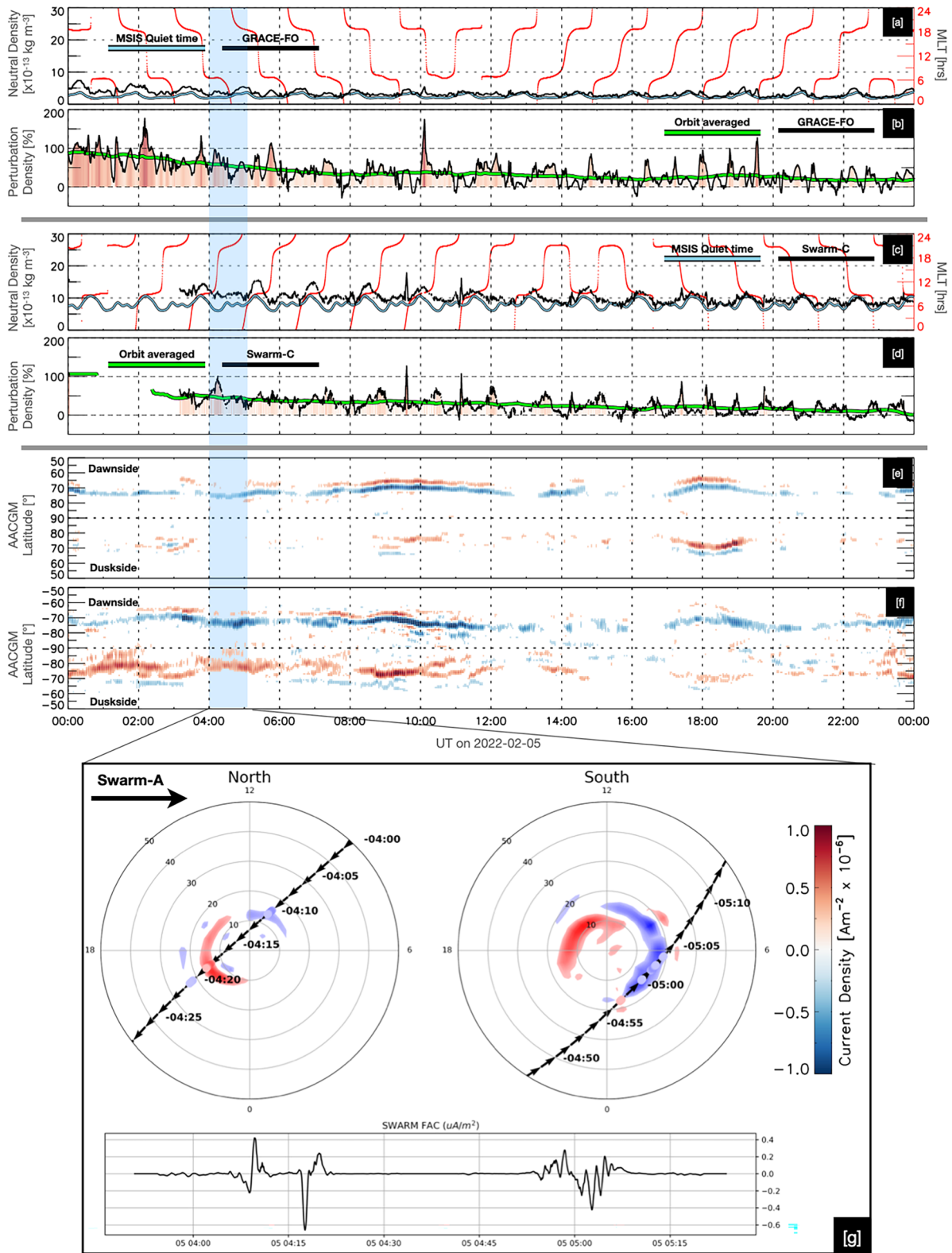


Figure 5. Same format as Figure 3, but for 5th February 2022.

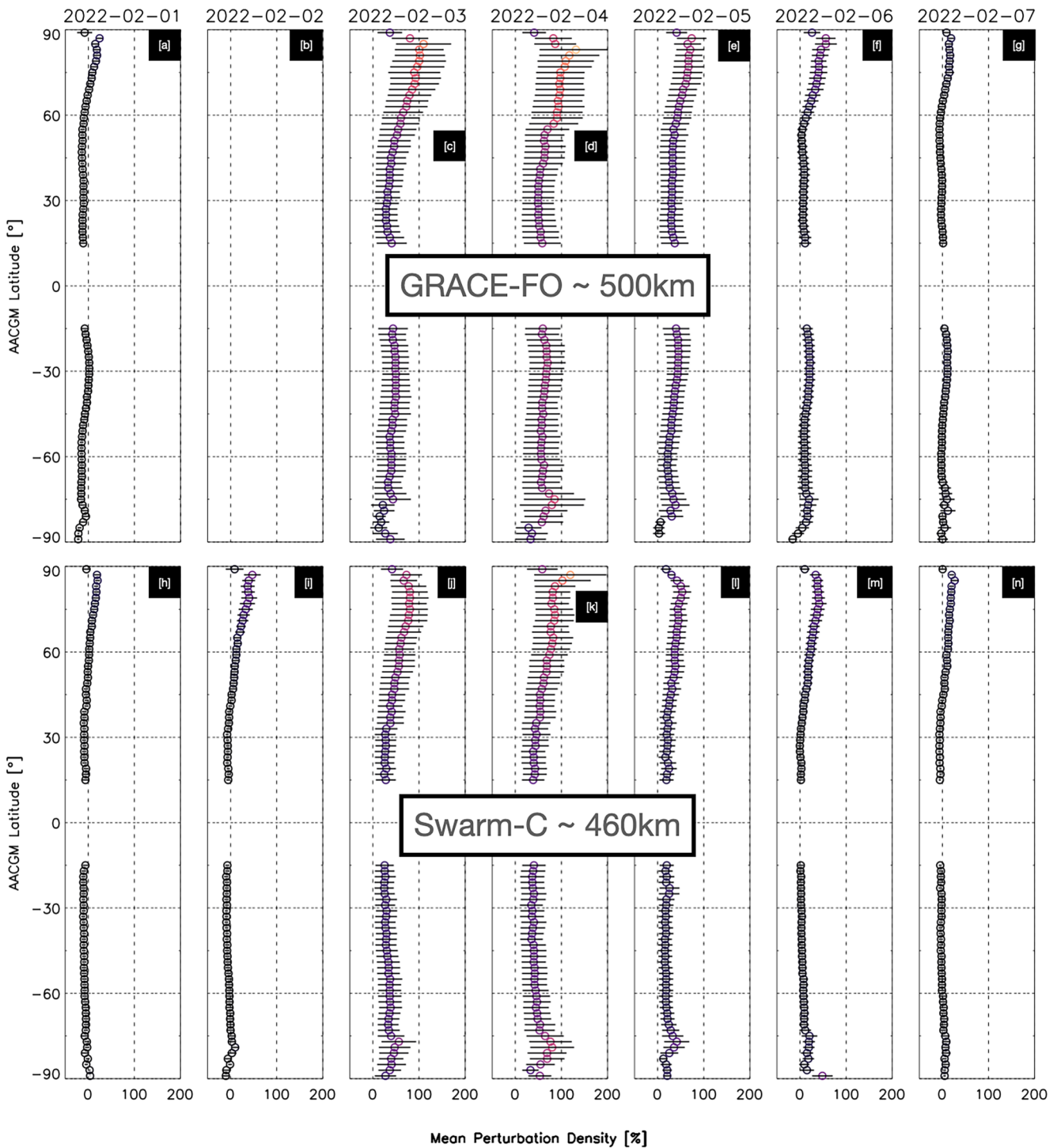


Figure 6. Latitude profiles of the mean thermospheric density from GRACE-FO (a–g) and Swarm C (h–n), for 1st–7th February 2022. Horizontal lines indicate the standard deviation of the mean for each latitude.

et al., 2019). We thus cannot in this study conclusively link AMPERE or Swarm measurements to Joule heating and density enhancements in the cusp. Various simulation studies have, however, shown this to be the case (e.g., Meng et al., 2022; Oigawa et al., 2022).

It is noted there were also discernible high latitude perturbations on average during the 2 days before the first storm (Figures 6a–6h, and 6i), particularly in the northern hemisphere on 2 February 2022 (i), even though the

geomagnetic activity levels were low (Figure 1, SYM-H index). As MSIS is an empirical model that cannot capture event-driven neutral densities, and that the high-latitude ionosphere/thermosphere is never truly devoid of geomagnetic influence, it likely that MSIS underestimated the high-latitude neutral density to some degree on the “quiet” days prior to the 3 February storm. Following this underestimation, there is some small uncertainty (up to ~20%) in our definition of quiet-time high-latitude neutral densities throughout this paper.

4. Summary

We have presented an analysis of the ionosphere-thermosphere conditions which lead to the loss of Starlink internet satellites in February 2022. Discrete geomagnetic storms on the 3rd and 4th February drove increases of the thermospheric mass density, increasing drag on the satellites and leading them to de-orbit on the 7th.

Utilizing newly processed high-resolution thermospheric density measurements from Swarm C and GRACE-FO, we have gained new insights into the global extent of density enhancements due to high-latitude ionospheric driving (captured by AMPERE and Swarm A FAC measurements). In particular:

- Thermospheric densities become enhanced globally, but are largest in the high-latitude polar regions above 80° AACGM latitude. The latitudinal distribution of the density perturbations is consistent with magnetospheric energy input into the cusp.
- Density perturbations between the northern and southern hemispheres were more symmetric on the 4th compared to the 3rd. This is consistent with the FAC data from AMPERE, which likewise exhibits stronger hemispherical symmetry on the 4th compared to the 3rd of February.
- Thermospheric density e-folding decay timescales in the auroral zones of both hemispheres were approximately 12 hr, except for Swarm C in the northern hemisphere, which was around 13 hr. The magnitude and extent of FACs reduced much quicker.
- The perturbation thermospheric density on the 4th appears to saturate, with its peak occurring 1–2 hr before the maximum excursion of SYM-H. This may be due to the very long main phase of the 4th of February storm, which lasted around 20 hr.

This study emphasizes the importance of capturing high-latitude ionospheric conditions when considering the impact of geomagnetic storms on the thermosphere, which can have dire consequences for LEO assets. These thermospheric storm effects are global in their extent and complex in their growth and decay, whilst their drivers are confined to high latitudes. There is additionally a complex thermospheric interplay between hemispheres, as ionospheric conditions in each can be highly asymmetric. For future analysis and potential real-time monitoring to support LEO satellite launches, capturing the high-latitude ionosphere is imperative. This monitoring could come in the form of real-time FAC streaming from LEO satellites with magnetometers, or perhaps more realistically, nowcasting of the high-latitude ionospheric convection, aurora, total electron content (TEC), magnetic perturbations from various ground-based instrumentation. The Super Dual Auroral Radar Network (SuperDARN), for example, includes several high-frequency radars that measure ionospheric plasma velocities in real-time (<https://superdarn.ca/real-time>), and several sources provide GNSS derived near-real-time TEC maps (e.g., <https://impc.dlr.de/products/total-electron-content/>). Rapid enhancements to both ionospheric velocities and TEC indicate geomagnetic storms and can be used in addition to geomagnetic indices, such as SYM-H, to more accurately anticipate the magnitude of thermospheric density enhancements (e.g., Billett et al., 2021; Jee et al., 2005).

Data Availability Statement

Data from the ESA Swarm A and C satellites, as well as GRACE-FO, was obtained from <https://swarm-diss.eo.esa.int>. AMPERE data can be plotted and downloaded at <http://ampere.jhuapl.edu/>. The NRLMSIS 2.0 model Fortran code was obtained from <https://map.nrl.navy.mil/map/pub/nrl/NRLMSIS/NRLMSIS2.0/>.

References

- Anderson, B. J., Korth, H., Waters, C. L., Green, D. L., Merkin, V. G., Barnes, R. J., & Dyrud, L. P. (2014). Development of large-scale Birkeland currents determined from the active magnetosphere and planetary electrodynamics response experiment. *Geophysical Research Letters*, *41*(9), 3017–3025. <https://doi.org/10.1002/2014gl059941>
- Anderson, B. J., Olson, C. N., Korth, H., Barnes, R. J., Waters, C. L., & Vines, S. K. (2018). Temporal and spatial development of global Birkeland currents. *Journal of Geophysical Research: Space Physics*, *123*(6), 4785–4808. <https://doi.org/10.1029/2018ja025254>

Acknowledgments

This research was supported by the European Space Agency (ESA) Living Planet Fellowship programme and by the National Sciences and Engineering Research Council of Canada (NSERC). DDB was supported by ESA under the “HLPF-SSA” project and by NSERC under CREATE Grant 479771-20. KM was supported by NSERC Discovery Grant RGPIN 05472-2017.

- Berger, T. E., Dominique, M., Lucas, G., Pilinski, M., Ray, V., Sewell, R., et al. (2023). The thermosphere is a drag: The 2022 Starlink incident and the threat of geomagnetic storms to low Earth orbit space operations. *Space Weather*, 21(3), e2022SW003330. <https://doi.org/10.1029/2022sw003330>
- Bezdek, A., Sebera, J., & Klokočník, J. (2018). Calibration of Swarm accelerometer data by GPS positioning and linear temperature correction. *Advances in Space Research*, 62(2), 317–325. <https://doi.org/10.1016/j.asr.2018.04.041>
- Billett, D. D., McWilliams, K. A., Pakhotin, I. P., Burchill, J. K., Knudsen, D. J., & Martin, C. J. (2022). High-resolution poynnting flux statistics from the swarm mission: How much is being underestimated at larger scales? *Journal of Geophysical Research: Space Physics*, 127(7), e2022JA030573. <https://doi.org/10.1029/2022ja030573>
- Billett, D. D., McWilliams, K. A., Perry, G. W., Clausen, L. B. N., & Anderson, B. J. (2022). Ionospheric energy input in response to changes in solar wind driving: Statistics from the SuperDARN and AMPERE campaigns. *Journal of Geophysical Research: Space Physics*, 127(3), e2021JA030102. <https://doi.org/10.1029/2021ja030102>
- Billett, D. D., McWilliams, K. A., Ponomarenko, P. V., Martin, C. J., Knudsen, D. J., & Vines, S. K. (2023). Multi-scale ionospheric poynnting fluxes using ground and space-based observations. *Geophysical Research Letters*, 50(10), e2023GL103733. <https://doi.org/10.1029/2023gl103733>
- Billett, D. D., Perry, G. W., Clausen, L. B. N., Archer, W. E., McWilliams, K. A., Haaland, S., et al. (2021). The relationship between large scale thermospheric density enhancements and the spatial distribution of poynnting flux. *Journal of Geophysical Research: Space Physics*, 126(5), e2021JA029205. <https://doi.org/10.1029/2021ja029205>
- Bruinsma, S., Tamagnan, D., & Biancale, R. (2004). Atmospheric densities derived from CHAMP/STAR accelerometer observations. *Planetary and Space Science*, 52(4), 297–312. <https://doi.org/10.1016/j.pss.2003.11.004>
- Cosgrove, R. B., Bahcivan, H., Chen, S., Sanchez, E., & Knipp, D. (2022). Violation of hemispheric symmetry in integrated poynnting flux via an empirical model. *Geophysical Research Letters*, 49(4), e2021GL097329. <https://doi.org/10.1029/2021gl097329>
- Cowley, S. W. H., & Lockwood, M. (1992). Excitation and decay of solar wind-driven flows in the magnetosphere-ionosphere system. *Annales Geophysicae*, 10, 103–115.
- Coxon, J. C., Shore, R. M., Freeman, M. P., Fear, R. C., Browett, S. D., Smith, A. W., et al. (2019). Timescales of Birkeland currents driven by the IMF. *Geophysical Research Letters*, 46(14), 7893–7901. <https://doi.org/10.1029/2018gl081658>
- Dang, T., Li, X., Luo, B., Li, R., Zhang, B., Pham, K., et al. (2022). Unveiling the space weather during the Starlink satellites destruction event on 4 February 2022. *Space Weather*, 20(8), e2022SW003152. <https://doi.org/10.1029/2022sw003152>
- Deng, Y., Maute, A., Richmond, A. D., & Roble, R. G. (2009). Impact of electric field variability on joule heating and thermospheric temperature and density. *Geophysical Research Letters*, 36(8). <https://doi.org/10.1029/2008gl036916>
- Doornbos, E. (2012). *Thermospheric density and wind determination from satellite dynamics*. Springer Science & Business Media.
- Dungey, J. W. (1961). Interplanetary magnetic field and the auroral zones. *Physical Review Letters*, 6(2), 47–48. <https://doi.org/10.1103/physrevlett.6.47>
- Emmert, J. T., Drob, D. P., Picone, J. M., Siskind, D. E., Jones, M., Jr., Mlynczak, M. G., et al. (2021). NRLMSIS 2.0: A whole-atmosphere empirical model of temperature and neutral species densities. *Earth and Space Science*, 8(3), e2020EA001321. <https://doi.org/10.1029/2020ea001321>
- Ercha, A., Ridley, A. J., Zhang, D., & Xiao, Z. (2012). Analyzing the hemispheric asymmetry in the thermospheric density response to geomagnetic storms. *Journal of Geophysical Research*, 117(8). <https://doi.org/10.1029/2011ja017259>
- Fang, T.-W., Kubaryk, A., Goldstein, D., Li, Z., Fuller-Rowell, T., Millward, G., et al. (2022). Space weather environment during the SpaceX Starlink satellite loss in February 2022. *Space Weather*, 20(11), e2022SW003193. <https://doi.org/10.1029/2022sw003193>
- Foster, J. C., St.-Maurice, J.-P., & Abreu, V. J. (1983). Joule heating at high latitudes. *Journal of Geophysical Research*, 88(A6), 4885–4897. <https://doi.org/10.1029/ja088ia06p04885>
- Friis-Christensen, E., Lühr, H., Knudsen, D., & Haagmans, R. (2008). Swarm—an Earth observation mission investigating geospace. *Advances in Space Research*, 41(1), 210–216. <https://doi.org/10.1016/j.asr.2006.10.008>
- Haggood, M., Liu, H., & Lugaz, N. (2022). SpaceX—Sailing close to the space weather? *Wiley Online Library*, 20(3).
- He, C., Yang, Y., Carter, B., Kerr, E., Wu, S., Deleflie, F., et al. (2018). Review and comparison of empirical thermospheric mass density models. *Progress in Aerospace Sciences*, 103, 31–51. <https://doi.org/10.1016/j.paerosci.2018.10.003>
- Hong, Y., Deng, Y., Zhu, Q., Maute, A., Hairston, M. R., Waters, C., et al. (2023). Inter-hemispheric asymmetries in high-latitude electrodynamic forcing and the thermosphere during the October 8–9, 2012, geomagnetic storm: An integrated data–model investigation. *Frontiers in Astronomy and Space Sciences*, 10, 1062265. <https://doi.org/10.3389/fspas.2023.1062265>
- Huang, C. Y., Huang, Y., Su, Y.-J., Hairston, M. R., & Sotirelis, T. (2017). DMSP observations of high latitude poynnting flux during magnetic storms. *Journal of Atmospheric and Solar-Terrestrial Physics*, 164, 294–307. <https://doi.org/10.1016/j.jastp.2017.09.005>
- Huang, C. Y., Su, Y.-J., Sutton, E. K., Weimer, D. R., & Davidson, R. L. (2014). Energy coupling during the August 2011 magnetic storm. *Journal of Geophysical Research: Space Physics*, 119(2), 1219–1232. <https://doi.org/10.1002/2013ja019297>
- Huang, Y., Richmond, A. D., Deng, Y., & Roble, R. (2012). Height distribution of joule heating and its influence on the thermosphere. *Journal of Geophysical Research*, 117(A8). <https://doi.org/10.1029/2012ja017885>
- Hutchinson, J. A., Wright, D. M., & Milan, S. E. (2011). Geomagnetic storms over the last solar cycle: A superposed epoch analysis. *Journal of Geophysical Research*, 116(A9). <https://doi.org/10.1029/2011ja016463>
- Iijima, T., & Potemra, T. A. (1978). Large-scale characteristics of field-aligned currents associated with substorms. *Journal of Geophysical Research*, 83(A2), 599–615. <https://doi.org/10.1029/ja083ia02p00599>
- long, D., Chen, Y., Toth, G., Zou, S., Pulkkinen, T., Ren, J., et al. (2022). New findings from explainable SYM-H forecasting using gradient boosting machines. *Space Weather*, 20(8), e2021SW002928. <https://doi.org/10.1029/2021sw002928>
- Iorffida, E., Daras, I., Haagmans, R., & Strømme, A. (2023). Swarm A and C accelerometers: Data validation and scientific interpretation. *Earth and Space Science*, 10(2). <https://doi.org/10.1029/2022ea002458>
- Jee, G., Schunk, R. W., & Scherliess, L. (2005). On the sensitivity of total electron content (TEC) to upper atmospheric/ionospheric parameters. *Journal of Atmospheric and Solar-Terrestrial Physics*, 67(11), 1040–1052. <https://doi.org/10.1016/j.jastp.2005.04.001>
- Joselyn, J. A. (1989). Geomagnetic quiet day selection. *Pure and Applied Geophysics*, 131(3), 333–341. <https://doi.org/10.1007/bf00876832>
- Knipp, D. J., Eriksson, S., Kilcommons, L., Crowley, G., Lei, J., Hairston, M., & Drake, K. (2011). Extreme poynnting flux in the dayside thermosphere: Examples and statistics. *Geophysical Research Letters*, 38(16). <https://doi.org/10.1029/2011gl048302>
- Knipp, D. J., Pette, D. V., Kilcommons, L. M., Isaacs, T. L., Cruz, A. A., Mlynczak, M. G., et al. (2017). Thermospheric nitric oxide response to shock-led storms. *Space Weather*, 15(2), 325–342. <https://doi.org/10.1002/2016sw001567>
- Kornfeld, R. P., Arnold, B. W., Gross, M. A., Dahya, N. T., Klipstein, W. M., Gath, P. F., & Bettadpur, S. (2019). GRACE-FO: The gravity recovery and climate experiment follow-on mission. *Journal of Spacecraft and Rockets*, 56(3), 931–951. <https://doi.org/10.2514/1.a34326>
- Laskar, F. I., Sutton, E. K., Lin, D., Greer, K. R., Aryal, S., Cai, X., et al. (2023). Thermospheric temperature and density variability during 3–4 February 2022 minor geomagnetic storm. *Space Weather*, 21(4), e2022SW003349. <https://doi.org/10.1029/2022sw003349>

- Leger, J.-M., Bertrand, F., Jager, T., Le Prado, M., Fratter, I., & Lalaurie, J.-C. (2009). Swarm absolute scalar and vector magnetometer based on helium 4 optical pumping. *Procedia Chemistry*, 1(1), 634–637. <https://doi.org/10.1016/j.proche.2009.07.158>
- Licata, R. J., Mehta, P. M., Weimer, D. R., Drob, D. P., Tobiska, W. K., & Yoshii, J. (2022). Science through machine learning: Quantification of post-storm thermospheric cooling. *Space Weather*, 20(9), e2022SW003189. <https://doi.org/10.1029/2022sw003189>
- Lin, D., Wang, W., Garcia-Sage, K., Yue, J., Merkin, V., McInerney, J. M., et al. (2022). Thermospheric neutral density variation during the “SpaceX” storm: Implications from physics-based whole geospace modeling. *Space Weather*, 20(12), e2022SW003254. <https://doi.org/10.1029/2022sw003254>
- Liu, H., Lühr, H., Henize, V., & Köhler, W. (2005). Global distribution of the thermospheric total mass density derived from CHAMP. *Journal of Geophysical Research*, 110(A4). <https://doi.org/10.1029/2004ja010741>
- Liu, R., Lühr, H., & Ma, S.-Y. (2010). Storm-time related mass density anomalies in the polar cap as observed by CHAMP. *Annales Geophysicae*, 28(1), 165–180. <https://doi.org/10.5194/angeo-28-165-2010>
- Lomidze, L., Burchill, J. K., Knudsen, D. J., Kouznetsov, A., & Weimer, D. R. (2019). Validity study of the swarm horizontal cross-track ion drift velocities in the high-latitude ionosphere. *Earth and Space Science*, 6(3), 411–432. <https://doi.org/10.1029/2018ea000546>
- Lotko, W., & Zhang, B. (2018). Alfvénic heating in the cusp ionosphere-thermosphere. *Journal of Geophysical Research: Space Physics*, 123(12), 10–368. <https://doi.org/10.1029/2018ja025990>
- Lu, G., Richmond, A. D., Lühr, H., & Paxton, L. (2016). High-latitude energy input and its impact on the thermosphere. *Journal of Geophysical Research: Space Physics*, 121(7), 7108–7124. <https://doi.org/10.1002/2015ja022294>
- Lühr, H., Park, J., Gjerloev, J. W., Rauberg, J., Michaelis, I., Merayo, J. M. G., & Brauer, P. (2015). Field-aligned currents’ scale analysis performed with the swarm constellation. *Geophysical Research Letters*, 42(1), 1–8. <https://doi.org/10.1002/2014gl062453>
- Lühr, H., Rother, M., Köhler, W., Ritter, P., & Grunwaldt, L. (2004). Thermospheric up-welling in the cusp region: Evidence from CHAMP observations. *Geophysical Research Letters*, 31(6). <https://doi.org/10.1029/2003gl019314>
- March, G., Van Den Ijssel, J., Siemes, C., Visser, P. N., Doornbos, E. N., & Pilinski, M. (2021). Gas-surface interactions modelling influence on satellite aerodynamics and thermosphere mass density. *Journal of Space Weather and Space Climate*, 11, 54. <https://doi.org/10.1051/swsc/2021035>
- McCullough, C. M., Harvey, N., Save, H., & Bandikova, T. (2019). Description of calibrated GRACE-FO accelerometer data products (ACT). In *Level-1 product version, 4*.
- Mehta, P. M., Walker, A. C., Sutton, E. K., & Godinez, H. C. (2017). New density estimates derived using accelerometers on board the CHAMP and GRACE satellites. *Space Weather*, 15(4), 558–576. <https://doi.org/10.1002/2016sw001562>
- Meng, X., Ozturk, D. S., Verkholjadova, O. P., Varney, R. H., Reimer, A. S., Semeter, J. L., et al. (2022). Energy deposition by mesoscale high-latitude electric fields into the thermosphere during the 26 October 2019 geomagnetic storm. *Journal of Geophysical Research: Space Physics*, 127(12), e2022JA030716. <https://doi.org/10.1029/2022ja030716>
- Newton, G. P., & Pelz, D. T. (1973). Neutral thermosphere temperatures from density scale height measurements. *Journal of Geophysical Research*, 78(4), 725–732. <https://doi.org/10.1029/ja078i004p00725>
- Oigawa, T., Shinagawa, H., & Taguchi, S. (2022). Two-dimensional local modeling of thermospheric heating and neutral mass density enhancement driven by Alfvén waves. *Journal of Geophysical Research: Space Physics*, 127(11), e2021JA030189. <https://doi.org/10.1029/2021ja030189>
- Oliveira, D. M., & Zesta, E. (2019). Satellite orbital drag during magnetic storms. *Space Weather*, 17(11), 1510–1533. <https://doi.org/10.1029/2019sw002287>
- Pakhotin, I. P., Mann, I. R., Xie, K., Burchill, J. K., & Knudsen, D. J. (2021). Northern preference for terrestrial electromagnetic energy input from space weather. *Nature Communications*, 12(1), 199. <https://doi.org/10.1038/s41467-020-20450-3>
- Pham, K. H., Zhang, B., Sorathia, K., Dang, T., Wang, W., Merkin, V., et al. (2022). Thermospheric density perturbations produced by traveling atmospheric disturbances during August 2005 storm. *Journal of Geophysical Research: Space Physics*, 127(2), e2021JA030071. <https://doi.org/10.1029/2021ja030071>
- Prölss, G. W. (2011). Density perturbations in the upper atmosphere caused by the dissipation of solar wind energy. *Surveys in Geophysics*, 32(2), 101–195. <https://doi.org/10.1007/s10712-010-9104-0>
- Prölss, G. W., & Očko, M. (2000). Propagation of upper atmospheric storm effects towards lower latitudes. *Advances in Space Research*, 26(1), 131–135. [https://doi.org/10.1016/s0273-1177\(99\)01039-x](https://doi.org/10.1016/s0273-1177(99)01039-x)
- Richardson, I. G., & Cane, H. V. (2012). Solar wind drivers of geomagnetic storms during more than four solar cycles. *Journal of Space Weather and Space Climate*, 2, A01. <https://doi.org/10.1051/swsc/2012001>
- Shepherd, S. G. (2014). Altitude-adjusted corrected geomagnetic coordinates: Definition and functional approximations. *Journal of Geophysical Research: Space Physics*, 119(9), 7501–7521. <https://doi.org/10.1002/2014ja020264>
- Shi, Y., Zesta, E., Connor, H. K., Su, Y.-J., Sutton, E. K., Huang, C. Y., et al. (2017). High-latitude thermosphere neutral density response to solar wind dynamic pressure enhancement. *Journal of Geophysical Research: Space Physics*, 122(11), 11–559. <https://doi.org/10.1002/2017ja023889>
- Siemes, C., Borries, C., Bruinsma, S., Fernandez-Gomez, I., Hladczuk, N., den Ijssel, J., et al. (2023). New thermosphere neutral mass density and crosswind datasets from CHAMP, GRACE, and GRACE-FO. *Journal of Space Weather and Space Climate*, 13, 16. <https://doi.org/10.1051/swsc/2023014>
- Siemes, C., deTeixeira da Encarnação, J., Doornbos, E., Van Den Ijssel, J., Kraus, J., Perešty, R., et al. (2016). Swarm accelerometer data processing from raw accelerations to thermospheric neutral densities. *Earth Planets and Space*, 68, 1–16. <https://doi.org/10.1186/s40623-016-0474-5>
- Tapley, B. D., Bettadpur, S., Watkins, M., & Reigber, C. (2004). The gravity recovery and climate experiment: Mission overview and early results. *Geophysical Research Letters*, 31(9). <https://doi.org/10.1029/2004gl019920>
- van den Ijssel, J., Doornbos, E., Iorfida, E., March, G., Siemes, C., & Montenbruck, O. (2020). Thermosphere densities derived from Swarm GPS observations. *Advances in Space Research*, 65(7), 1758–1771. <https://doi.org/10.1016/j.asr.2020.01.004>
- Visser, P. N. A. M., & van den Ijssel, J. (2016). Calibration and validation of individual GOCE accelerometers by precise orbit determination. *Journal of Geodesy*, 90, 1–13. <https://doi.org/10.1007/s00190-015-0850-0>
- Wang, X., Miao, J., Lu, X., Aa, E., Liu, J., Wang, Y., & Liu, S. (2021). Latitudinal impacts of joule heating on the high-latitude thermospheric density enhancement during geomagnetic storms. *Journal of Geophysical Research: Space Physics*, 126(7), e2020JA028747. <https://doi.org/10.1029/2020ja028747>
- Waters, C. L., Anderson, B. J., Green, D. L., Korth, H., Barnes, R. J., & Vanhamäki, H. (2020). Science data products for AMPERE. In *Iono-spheric multi-spacecraft analysis tools: Approaches for deriving ionospheric parameters* (pp. 141–165).
- Weimer, D. R., Mehta, P. M., Licata, R. J., & Tobiska, W. K. (2023). Global variations in the time delays between polar ionospheric heating and the neutral density response. *Space Weather*, 21(4), e2022SW003410. <https://doi.org/10.1029/2022sw003410>
- Yokoyama, N., & Kamide, Y. (1997). Statistical nature of geomagnetic storms. *Journal of Geophysical Research*, 102(A7), 14215–14222. <https://doi.org/10.1029/97ja00903>

- Zesta, E., & Oliveira, D. M. (2019). Thermospheric heating and cooling times during geomagnetic storms, including extreme events. *Geophysical Research Letters*, *46*(22), 12739–12746. <https://doi.org/10.1029/2019gl085120>
- Zhou, Y.-L., Ma, S.-Y., Lühr, H., Wang, H., & Dang, G. (2007). Changes of thermospheric mass density and their relations with Joule heating and ring current index during Nov. 2003 Superstorm—CHAMP observations. *Chinese Journal of Geophysics*, *50*(4), 856–865.
- Zhu, Q., Lu, G., Lei, J., Deng, Y., Doornbos, E., van den IJssel, J., & Siemes, C. (2023). Interhemispheric asymmetry of the thermospheric neutral density response to the 7–9 September 2017 geomagnetic storms. *Geophysical Research Letters*, *50*(11), e2023GL103208. <https://doi.org/10.1029/2023gl103208>